Supporting information

Polythiophene as efficient mediator to anchor in-situ grown Ni hydroxide cluster for urea oxidation reaction.

Shi-Jie Lu[a], Hao-Nan Li[a], Kai Wei[a], Weijia Song[a,b], Hsiao-Chien Chen[c] and Nian-Tzu Suen[,a,b,c,d]*

a. Institute of Innovation Materials and Energy, College of Chemistry & Chemical Engineering, Yangzhou University, Yangzhou 225002, China

b. Yangzhou High School, Yangzhou, Jiangsu, 225009, China

c. Dual Master Program in Nano-Electronic Engineering and Design; Center for Sustainability and Energy Technologies, Chang Gung University, Taoyuan 33302, Taiwan.

d. Yunnan Key Laboratory of Electromagnetic Materials and Devices, Yunnan University, Kunming 650500, P. R. China.

e. State Key Laboratory of Structural Chemistry, Fujian Institute of Research on the Structure of Matter, Chinese Academy of Sciences, Fuzhou, 350002, P. R. China

f. Jiangsu Provincial Key Laboratory of Green & Functional Materials and Environmental Chemistry, Yangzhou 225002, China

Experimental part

Experimental chemical reagents

The nickel powder (Ni, 99.5%), tetrabutylammonium perchlorate (TBAP, 99%), nickel chloride hexahydrate (99.9%), potassium hydroxide (ACS grade), and urea (99%) used for material synthesis and electrochemical testing were purchased from Aladdin Reagent Company. Dichloromethane (DCM, 99.5%), thiophene (98%), and relatively hydrophilic carbon cloth (model W0S1011) were sourced from Shanghai Titan Scientific Co., Ltd., TCI (Shanghai) Chemical Industry Development Co., Ltd., and Suzhou Sinero Technology Co., Ltd., respectively. Chemical reagents required for material characterization, including sulfuric acid (98%), hydrogen peroxide (30%), hydrochloric acid (31%), nitric acid (68%), and ammonium fluoride (99.8%), were supplied by Sinopharm Chemical Reagent Co., Ltd.

Preparation of working electrodes

Four types of working electrodes were prepared. The first type was prepared by compressing 50 mg of nickel powder into a pellet (8 mm in diameter), which was directly employed as the working electrode. The second type, designated as Ni^{2+}@CC, was prepared by dissolving 30 mg of nickel chloride hexahydrate in 30 mL of secondary water to obtain a nickel ion solution. A piece of carbon cloth (1 × 1 cm^2) was immersed in this solution using an electrode clip and stirred for 20 hours to obtain the Ni^{2+}@CC working electrode. The third working electrode, designated as Ni^{2+}@PTh@CC, was synthesized using an electrochemical workstation (CHI660e, Shanghai Chenhua Instrument Co., Ltd.) via an electrochemical polymerization process within a nitrogen-filled glove box. Initially, a 0.4 mol/L thiophene solution was prepared by dissolving 1.7095 g of tetrabutylammonium perchlorate (TBAP) in a portion of dichloromethane (DCM), adding 3.2 mL of thiophene, and diluting the mixture to 100 mL with DCM. Electropolymerization was carried out using a standard three-electrode system, with carbon cloth (1 × 1 cm^2) as the working

electrode, a platinum sheet (1 × 1 cm^2) as the counter electrode, and a saturated calomel electrode (SCE) as the reference electrode. Cyclic voltammetry (CV) scans were performed within a potential range of 0 V to 2.0 V (vs. SCE) at a scan rate of 5 mV/s for 40 consecutive cycles to obtain polythiophene (PTh@CC). Finally, the prepared polythiophene (PTh@CC) was fixed with an electrode clip, immersed in a nickel ion solution, and stirred for 20 hours to obtain the Ni^{2+}@PTh@CC working electrode. The fourth working electrode, denoted as PTh@CC, was prepared by using the third electrode as the working electrode without Ni^{2+} adsorption.

Additionally, three other different types of working electrodes were prepared: first, working electrodes based on PTh@CC adsorbed with 0.001 M Ni^{2+} and 0.1 M Ni^{2+}, respectively; second, working electrodes utilizing nickel foam of varying thicknesses; and finally, working electrodes fabricated by synthesizing $Ni(OH)_2$@CC via a hydrothermal method.[1]

Characterization

The crystal structure, phase distribution, and crystallinity of the prepared working electrode materials were analyzed using powder X-ray diffraction (PXRD, Bruker D8 Advance, Cu $k_{\alpha1}$: 1.54056 Å) with a scanning range of 20–60° and a scanning rate of 5°/min. The valence states of the corresponding elements (C, N, O, Ni, S) in the working electrode materials were analyzed by X-ray photoelectron spectroscopy (XPS, Thermo Scientific ESCALAB 250Xi). The main functional groups involved in the reaction were detected using an in-situ Fourier transform infrared spectrometer (Thermo Scientific™ Nicolet™ iS50 FTIR) and a Nicolet iS20 FTIR spectrometer, and their evolutionary behavior and formation mechanisms were investigated. Intermediate products generated during the reaction process were detected using an ultraviolet-visible spectrophotometer (UV-1280).

Electrochemical measurement

The electrochemical tests in this work were conducted using

electrochemical workstations from Jiangsu Donghua Analytical Instrument Co., Ltd. (model DH7006) and Shanghai Chenhua Instrument Co., Ltd. (model CHI660e). A standard three-electrode system was employed, with a platinum sheet electrode as the counter electrode and a saturated calomel electrode as the reference electrode. All electrochemical tests were performed in 1.0 M KOH and 1.0 M KOH containing 0.33 M $CO(NH_2)_2$ electrolytes. The three prepared working electrodes were tested for the oxygen evolution reaction and urea oxidation reaction. The measured potentials were converted to the reversible hydrogen electrode (RHE) scale and compensated for 90% of the ohmic voltage drop (R_u).

$$E_{RHE} = E_{ref} + 0.05916 * pH - 0.9 * I * R_u$$

Cyclic voltammetry (CV) tests were performed within a voltage range of 0.1 V to 0.15 V (vs. SCE). Five CV curves were obtained at different scan rates (20 mV/s, 40 mV/s, 60 mV/s, 80 mV/s, and 100 mV/s), enabling the calculation of the roughness factor (RF) and electrochemical active surface area (ECSA) for different materials, thereby eliminating the influence of electrode surface area on performance.

Theoretical calculation

Atomic simulation environment (ASE) software with GPAW calculator was used to simulate the adsorbed Ni^{2+} ion on PTh and to compute the adsorption energy of cyanate anion (OCN^-) on the surface of both Ni metal and imaginary structure, $Ni(OH)_2$-NiC, for Ni^{2+}@PTh@CC.[2, 3] Slab with three atomic layers was set to be the initial model and 15 Å vacuum spacing is inserted between each slab. The top two layers and OCN^- adsorbate were allowed to relax during geometry optimization. The final structure was determined when the maximum force of was lower than 0.05 $eV•Å^{-1}$. The exchange-correlation energies of the systems were calculated using the revised Perdew-Burke-Ernzerhof (RPBE) functionals.[4]

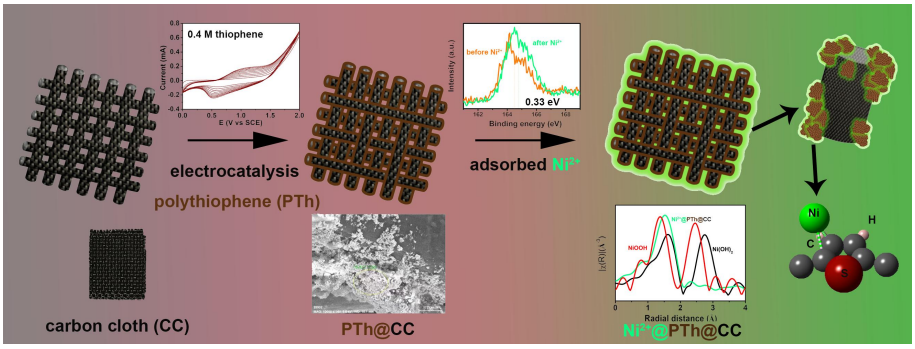

Figure S1. The synthetic flowchart of Ni^{2+}@PTh@CC composite electrode. Characterization results such as SEM image, XPS and XAS were also demonstrated to verify the synthetic process at each step.

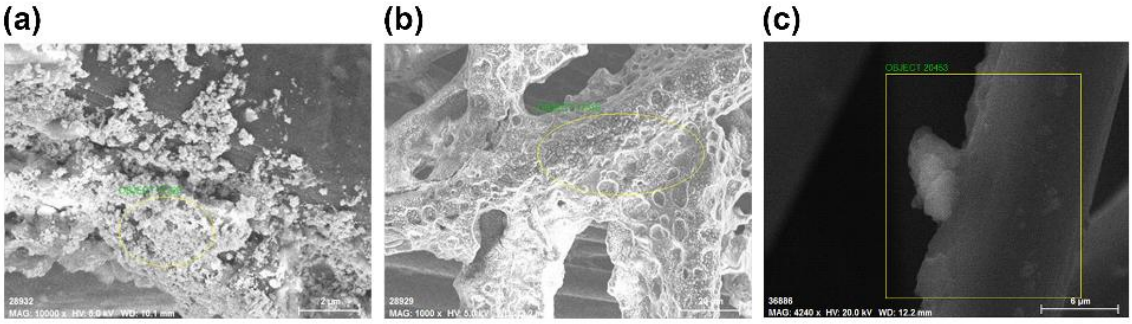

Figure S2. SEM of (a) PTh@CC and Ni^{2+}@PTh@CC (b) before and (c) after UOR.

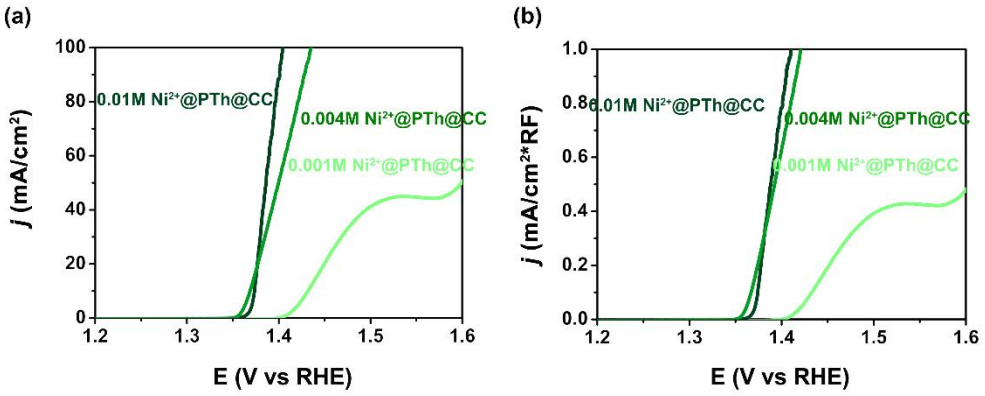

Figure S3. (a) LSV and (b) RF normalized LSV of 0.01M Ni^{2+}@PTh@CC and 0.004M Ni^{2+}@PTh@CC and 0.001M Ni^{2+}@PTh@CC composite electrodes in 1.0 M KOH containing 0.33 M $CO(NH_2)_2$.

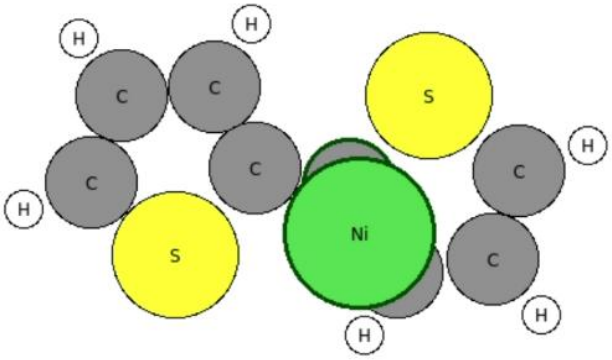

Figure S4. DFT calculation for the diagram of polythiophene adsorbing Ni^{2+}.

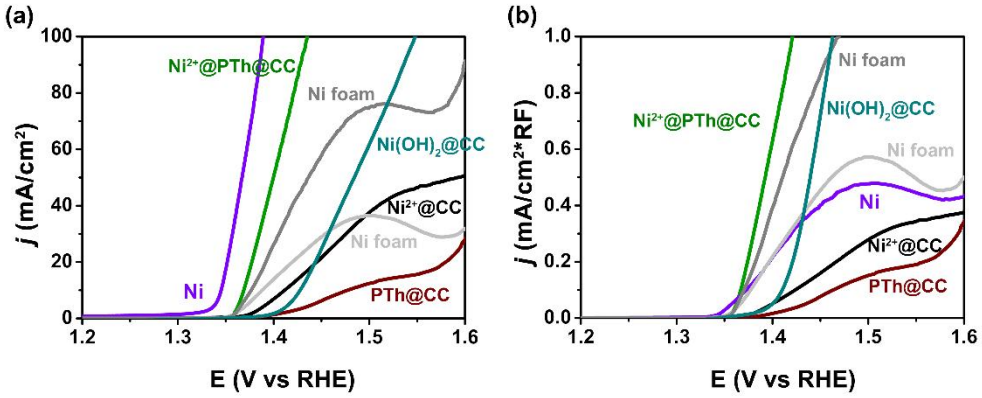

Figure S5. (a) LSV and (b) RF normalized LSV of Ni, Ni^{2+}@PTh@CC, Ni foam (light gray: 0.1 mm thick and dark gray: 1 mm thick), Ni^{2+}@CC, PTh@CC and $Ni(OH)_2$@CC composite electrodes in 1.0 M KOH containing 0.33 M $CO(NH_2)_2$.

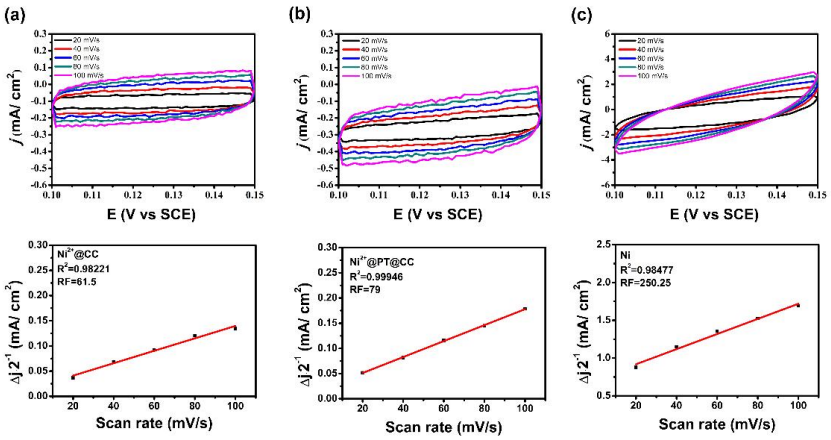

Figure S6. Cyclic voltammograms (CV) and linear regression slope derived from CV of (a) Ni^{2+}@CC, (b) Ni^{2+}@PTh@CC and (c) Ni in 1.0 M KOH.

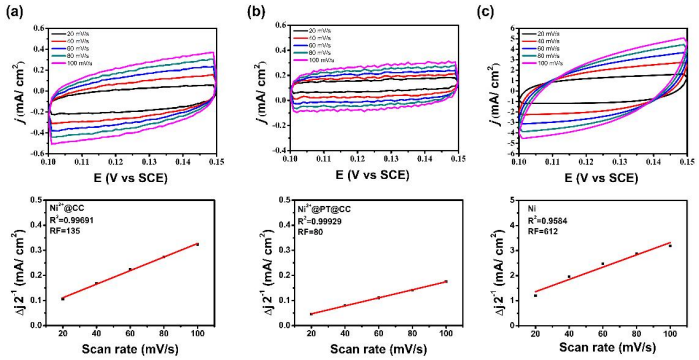

Figure S7. Cyclic voltammograms (CV) and linear regression slope derived from CV of (a) Ni^{2+}@CC, (b) Ni^{2+}@PTh@CC and (c) Ni in 1.0 M KOH containing 0.33 M $CO(NH_2)_2$.

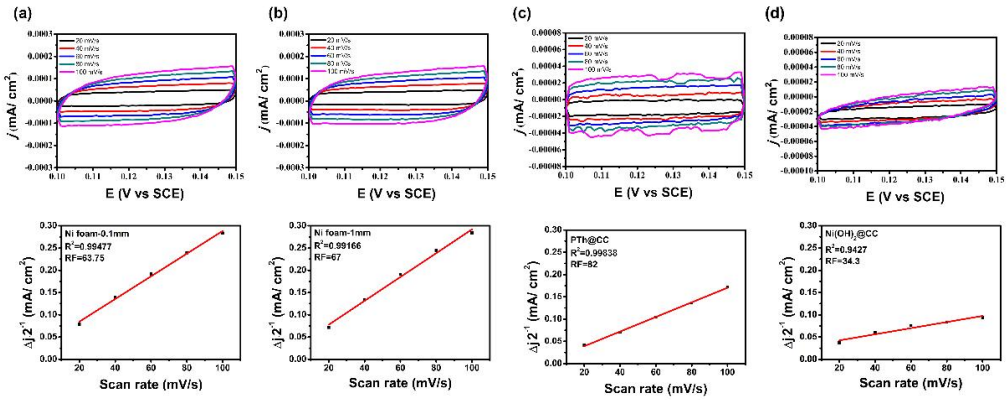

Figure S8. Cyclic voltammograms (CV) and linear regression slope derived from CV of (a) Ni foam (0.1 mm thick), (b) Ni foam (1 mm thick), (c) PTh@CC and (d) $Ni(OH)_2$@CC in 1.0 M KOH containing 0.33 M $CO(NH_2)_2$.

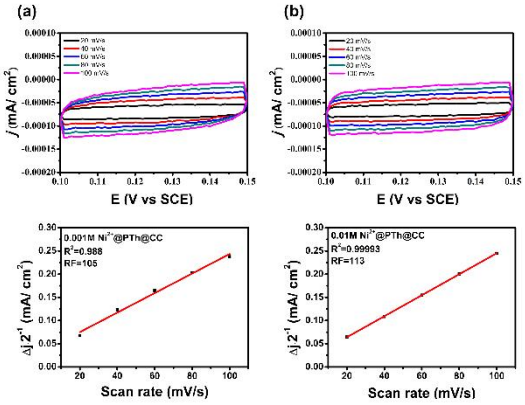

Figure S9. Cyclic voltammograms (CV) and linear regression slope derived from CV of (a) 0.001M Ni^{2+}@PTh@CC and (b) 0.01M Ni^{2+}@PTh@CC in 1.0 M KOH containing 0.33 M $CO(NH_2)_2$.

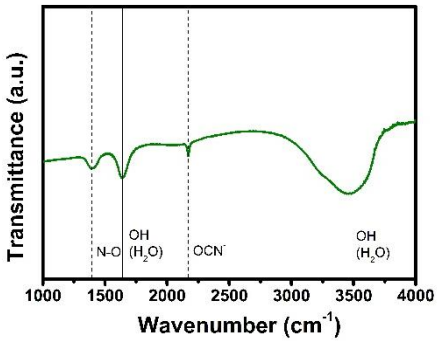

Figure S10. Nicolet iS20 FTIR spectra of Ni^{2+}@PTh@CC with droplet solution of 1.0 M KOH solution with 0.1 M KOCN without applied voltage.

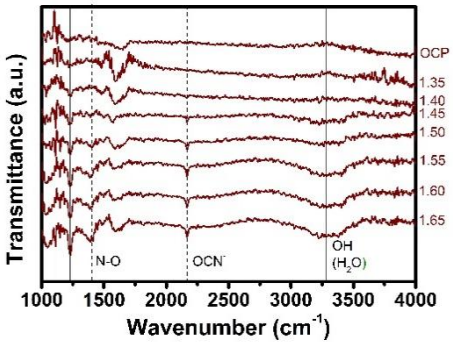

Figure S11. In situ FTIR spectra of PTh@CC from 1.35 to 1.65 V (V vs RHE) during UOR.

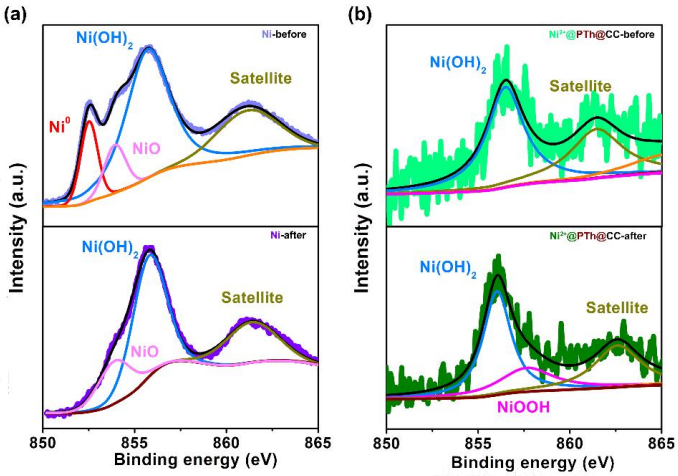

Figure S12. XPS spectra in the range of Ni 2p of Ni metal and Ni^{2+}@PTh@CC before/after UOR in 1.0 M KOH containing 0.33 M $CO(NH_2)_2$.

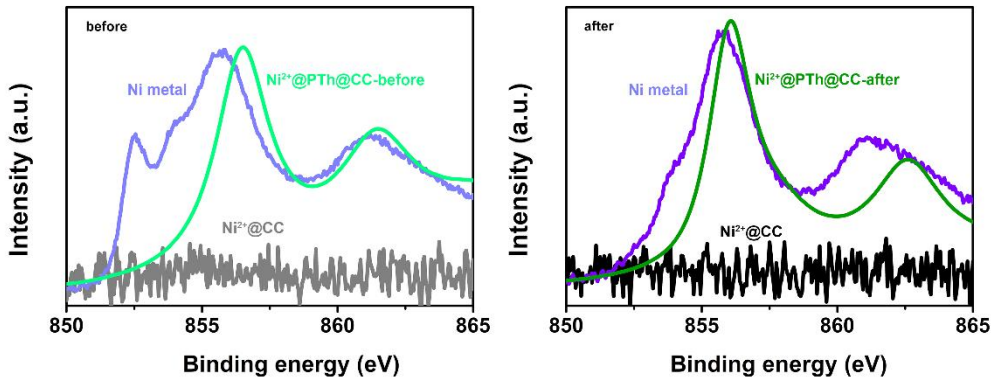

Figure S13. XPS in the regions of Ni 2p for Ni metal, Ni^{2+}@CC and Ni^{2+}@PTh@CC composite electrodes before and after UOR. XPS of Ni^{2+}@PTh@CC was replaced with fitted curve for the readers' convenience to compare Ni valence state before/ after UOR.

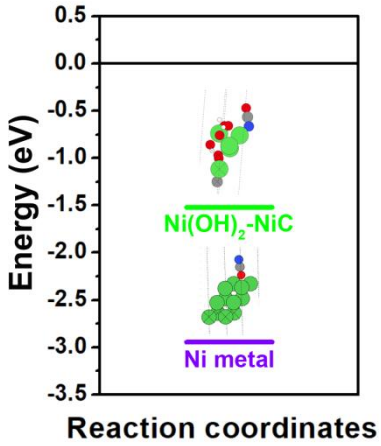

Figure S14. Calculated adsorption energy of cyanate anion (OCN^-) on the surface of Ni metal and imaginary structure, $Ni(OH)_2$-NiC, for Ni^{2+}@PTh@CC. Their theoretical models after structural optimization were also provided.

Table S1. The corresponding values of potential (j = 10 mA/cm^2) and Tafel slope of recent reported UOR electrocatalysts.

Samples	Potential/V (j = 10 mA/cm^2)	Tafel Slope (mV/ dec)	Ref
Ni	1.345	31.3	This work
NiF_3/Ni_2P@CC	1.36	33	[5]
Ni^{2+}@PTh@CC	1.368	34.4	This work
NiO–CrO@N–C	1.37	11.5	[6]
Fe_3O_4/NF	1.38	28	[7]

NiFe/NiFeCH/CC	1.39	/	[8]
VO_x/Ni/Ni_3N	1.40	/	[9]
CoS_2 NA/Ti	1.40	80	[10]
NiTe-$MoTe_2$	1.40	27.5	[11]
Ni^{2+}@CC	1.41	102	This work
Ni_2P/N-$C_{nanorods}$	1.41	36.7	[12]
NiCoP/CC	1.42	49	[13]
NiFe-LDH/CC	1.42	68	[14]
CoFe LDH/MOF-0.06	1.45	73.5	[15]
$NiCo_2O_4$/CC	1.45	75	[16]
$CoSe_2$/$MoSe_2$@CC	1.48	/	[17]
Co_3Mo_1S-CC	1.50	/	[18]
CrCoNiFe	1.62	74	[19]

REFERENCES

1. Ma, Y.; Yang, M.; Jin, X., Formation mechanisms for hierarchical nickel hydroxide microstructures hydrothermally prepared with different nickel salt precursors. *Colloids Surf. A* **2020**, *588*.
2. Lisesivdin, S. B.; Sarikavak-Lisesivdin, B., gpaw-tools – higher-level user interaction scripts for GPAW calculations and interatomic potential based structure optimization. *Comput. Mater. Sci* **2022,** *204*.
3. Enkovaara, J.; Rostgaard, C.; Mortensen, J. J.; Chen, J.; Dulak, M.; Ferrighi, L.; Gavnholt, J.; Glinsvad, C.; Haikola, V.; Hansen, H. A.; et al. Electronic structure calculations with GPAW: a real-space implementation of the projector augmented-wave method. *J Phys-Condens Mat* **2010**, *22* (25).
4. Hammer, B.; Hansen, L. B.; Nørskov, J. K., Improved adsorption energetics within density-functional theory using revised Perdew-Burke-Ernzerhof functionals. *Phys. Rev. B* **1999,** *59* (11), 7413-7421.
5. Wang, K.; Huang, W.; Cao, Q.; Zhao, Y.; Sun, X.; Ding, R.; Lin, W.; Liu, E.; Gao, P., Engineering NiF_3/Ni_2P heterojunction as efficient electrocatalysts for urea oxidation and splitting. *Chem. Eng. J.* **2022,** *427*.
6. Wu, N.; Chi, X.; Zhang, Y.; Hu, T., Convenient synthesis and enhanced urea oxidation of NiO–CrO@N–C. *New J. Chem.* **2024,** *48* (13), 5621-5626.
7. Bandal, H. A.; Kim, H., In situ construction of Fe_3O_4@FeOOH for efficient electrocatalytic urea oxidation. *Colloid Interface Sci.* **2022,** *627*, 1030-1038.
8. Wang, X.; Zhao, M.; Gong, Z.; Fang, S.; Hu, S.; Pi, W.; Bao, H., Cauliflower-like NiFe alloys anchored on a flake iron nickel carbonate hydroxide heterostructure towards superior overall water and urea electrolysis. *Nanoscale* **2023,** *15* (2), 779-790.
9. Wang, J.; Wang, C.; Zhang, X.; Li, S.; Yang, C.; Zhang, J., Interface Engineering of VOx/Ni/Ni_3N Heterostructures for Electrochemical Urea-Assisted Hydrogen Production. *Inorg. Chem.* **2024,** *63* (34), 15804-15812.
10. Wei, S.; Wang, X.; Wang, J.; Sun, X.; Cui, L.; Yang, W.; Zheng, Y.; Liu, J., CoS_2

nanoneedle array on Ti mesh: A stable and efficient bifunctional electrocatalyst for urea-assisted electrolytic hydrogen production. *Electrochim. Acta* **2017,** *246*, 776-782.

11. Yin, C.; Wang, S.; Yang, F.; Feng, L., Carbon-constrained heterogeneous Ni-Mo telluride for efficient urea oxidation. *Chin. Chem. Lett.* **2025**.
12. Zhang, X.; Ma, G.; Shui, L.; Zhou, G.; Wang, X., Urea electrooxidation-boosted hydrogen production on nitrogen-doped porous carbon nanorod-supported nickel phosphide nanoparticles. *Energy Chem.* **2022,** *72*, 88-96.
13. Sha, L.; Yin, J.; Ye, K.; Wang, G.; Zhu, K.; Cheng, K.; Yan, J.; Wang, G.; Cao, D., The construction of self-supported thorny leaf-like nickel-cobalt bimetal phosphides as efficient bifunctional electrocatalysts for urea electrolysis. *Mater. Chem. A* **2019,** *7* (15), 9078-9085.
14. Zhang, L.; Zhang, R.; Ge, R.; Ren, X.; Hao, S.; Xie, F.; Qu, F.; Liu, Z.; Du, G.; Asiri, A. M.; Zheng, B.; Sun, X., Facilitating Active Species Generation by Amorphous NiFe‐Bi Layer Formation on NiFe‐LDH Nanoarray for Efficient Electrocatalytic Oxygen Evolution at Alkaline pH. *Chem. Eur. J.* **2017,** *23* (48), 11499-11503.
15. Huang, S.; Wu, Y.; Fu, J.; Xin, P.; Zhang, Q.; Jin, Z.; Zhang, J.; Hu, Z.; Chen, Z., Hierarchical CoFe LDH/MOF nanorods array with strong coupling effect grown on carbon cloth enables efficient oxidation of water and urea. *Nanotechnology* **2021,** *32* (38).
16. Song, W.; Xu, M.; Teng, X.; Niu, Y.; Gong, S.; Liu, X.; He, X.; Chen, Z., Construction of self-supporting, hierarchically structured caterpillar-like $NiCo_2S_4$ arrays as an efficient trifunctional electrocatalyst for water and urea electrolysis. *Nanoscale* **2021,** *13* (3), 1680-1688.
17. Yang, Y.; Xiong, Y.; Yang, J.; Qian, D.; Chen, Y.; He, Y.; Hu, Z., Three-Dimensional Heterostructured $CoSe_2$/$MoSe_2$@CC as Trifunctional Electrocatalysts for Energy-Efficient Hydrogen Production. *Energy & Fuels* **2024,** *38* (3), 2260-2272.
18. Li, P.; Zhuang, Z.; Du, C.; Xiang, D.; Zheng, F.; Zhang, Z.; Fang, Z.; Guo, J.; Zhu, S.; Chen, W., Insights into the Mo-Doping Effect on the Electrocatalytic Performance of Hierarchical CoxMoyS Nanosheet Arrays for Hydrogen Generation and Urea Oxidation. *ACS Appl. Mater. Interfaces* **2020,** *12* (36), 40194-40203.
19. Liu, Q.; Zhao, P.; Zhao, F.; Zhu, J.; Yang, S.; Chen, L.; Zhang, Q., Bulk CrCoNiFe alloy with high conductivity and density of grain boundaries for oxygen evolution reaction and urea oxidation reaction. *Colloid Interface Sci.* **2023,** *644*, 1-9.